UNCECOMP 2015
1st ECCOMAS Thematic Conference on
Uncertainty Quantification in Computational Sciences and Engineering
M. Papadrakakis, V. Papadopoulos, G. Stefanou (eds.)
Crete Island, Greece, 25–27 May 2015

A POLYNOMIAL CHAOS METHOD FOR UNCERTAINTY QUANTIFICATION IN BLOOD PUMP SIMULATION

Michael Schick[1], **Chen Song**[1,2], **Vincent Heuveline**[1,2]

[1]Heidelberg Institute of Theoretical Studies
Data Mining and Uncertainty Quantification (DMQ) Group
Schloss-Wolfsbrunnenweg 35, 69118 Heidelberg, Germany
{michael.schick, chen.song, vincent.heuveline}@h-its.org

[2] Heidelberg University
Interdisciplinary Center for Scientific Computing (IWR)
Speyerer Str. 6, 69115 Heidelberg, Germany
{chen.song, vincent.heuveline}@uni-heidelberg.de

Keywords: Polynomial Chaos, stochastic Galerkin projection, Multiple Reference Frame, Uncertainty Quantification, Blood Pump, CFD.

Abstract. *Since the end of last century, ventricular assist devices (blood pumps) became one of the most common therapeutic instruments for the treatment of cardiac insufficiency, more than 23 million people are suffering from heart failure worldwide. To this end, computational fluid dynamics (CFD) is widely used in order to get insight into patient specific blood flow behaviour. Despite the fact that a great number of blood pumps are successfully used in practice, there are still many parameters within the CFD simulation, which face uncertainties due to, for example, variations in manufacturing processes or patient specific data. This makes uncertainty quantification an important tool in classical CFD analysis.*

We consider the Polynomial Chaos expansion with stochastic Galerkin projection in that context. It provides a powerful mean of computing the propagation of uncertainties at once by solution of one single deterministic, and coupled system. A part of the uncertainties we consider are of geometric type, which model an uncertain angular speed of the rotor segment of the pump. We adapt the Multiple Reference Frame method to map the rotation to a stationary reference system and transfer the geometric uncertainty to the Navier-Stokes equations as additional coriolis and centrifugal forces. We compare numerically a Krylov subspace method with mean based preconditioning against a multilevel Polynomial Chaos method for the solution of the governing equations, and verify our results against deterministic reference computations.

1 INTRODUCTION

Nowadays, medical devices have been undergoing a revolution and high-tech equipments are used for different purposes among the fields of health care. The innovation in biomedical devices in last decades grows significantly aiming at safer, more accurate and less invasive ways to treat patients. In this context, technical blood pumps became one of the most common therapeutic instruments for the treatment of cardiac insufficiency, e.g., replacing the pumping functionality of the human heart during surgery [2, 4, 9, 17, 25]. The verification and validation of such a device by numerical simulation is very difficult as it requires knowledge about various model parameters. These often face uncertainties, which may arise for example by variations in manufacturing processes or in patient specific blood characteristics.

In this paper, we analyse a blood pump model based on the incompressible Navier-Stokes equations with uncertain geometric and model specific parameters. The geometry is adapted from a benchmark problem of the U.S. Food and Drug Administration [1]. A part of the pump consists of a rotor with uncertain speed of rotation. Our goal is to map the geometric uncertainty to the model equations by making use of the Multiple Reference Frame (MRF) method from deterministic CFD [3, 6, 11, 13]. Thereby, the flow equations can be considered on a stationary reference domain, while the rotation is modeled by additional coriolis and centrifugal forces in the momentum equations. We consider the steady state Navier-Stokes equations for laminar flow with artificially decreased fluid density for stabilization. Although, in a more realistic scenario an instationary flow with a high Reynolds number needs to be assumed, our solution can serve as an initial guess, which significantly can improve convergence in the time-dependent case. Furthermore, our work provides insight into the use of efficient numerical methods for the MRF method with Uncertainty Quantification in fluid flow problems.

The spatial part is discretized by the finite element method. Assuming a point wise second order stochastic solution, spectral methods provide a powerful tool in case of a smooth dependence of the system response on the uncertain parameters. Polynomial Chaos (PC) expansions [10, 27] express the solution as a series of predefined random functionals without prior information on the probability law of the solution. The PC basis functionals are orthogonal multivariate polynomials in the random input variables whose probability distribution is defined *a priori*. The coefficients within the expansion need to be determined computationally. One popular approach is the use of non-intrusive methods, such as Monte Carlo or sparse-grid collocation [16]. An alternative, yet powerful approach is the stochastic Galerkin projection [10, 15], which we focus on in this work. It has been successfully applied to fluid flow problems with uncertain parameters, see e.g. [12, 14, 15, 22, 24]. The governing equations are projected on the space spanned by the Polynomial Chaos basis requiring the solution of a single fully coupled system. However, for that case the development of efficient preconditioners and solvers is a big challenge and is still in its infancy.

The remainder of this paper is structured in the following way. In Section 2 we introduce the model equations with uncertain parameters and show how the MRF method can be used to map the geometric uncertainty to the parameter space. Section 3 describes corresponding numerical solution methods, which we use for the numerical results presented in Section 4. We conclude this work and provide an outlook on open research questions in Section 5.

2 MODEL EQUATIONS

We consider the incompressible Navier-Stokes equations in steady state formulation using primitive variables $\vec{u}$ for velocity and p for pressure:

$$(\vec{u}(\vec{x}) \cdot \nabla)\vec{u}(\vec{x}) - \nu\Delta\vec{u}(\vec{x}) + \nabla p(\vec{x}) = 0, \qquad \vec{x} \in \mathcal{D}, \tag{1}$$

$$\nabla \cdot \vec{u}(\vec{x}) = 0, \qquad \vec{x} \in \mathcal{D}, \tag{2}$$

$$\vec{u}(\vec{x}) = \vec{g}(\vec{x}), \qquad \vec{x} \in \Gamma_i, \tag{3}$$

$$\vec{u}(\vec{x}) = 0, \qquad \vec{x} \in \Gamma_w \cup \Gamma_r, \tag{4}$$

$$\int_{\Gamma_o} \nu\nabla\vec{u}(\vec{x}) \cdot \vec{n}(\vec{x}) - p(\vec{x})\vec{n}(\vec{x})\, d\vec{x} = 0. \tag{5}$$

The flow is considered on $\mathcal{D} \subset \mathbb{R}^3$ with $\Gamma_i \subset \partial\mathcal{D}$ and $\Gamma_o \subset \partial\mathcal{D}$ defining the Dirichlet inflow and outflow boundary, respectively (compare Figure 1). At $\Gamma_w \cup \Gamma_r$ we prescribe no-slip boundary conditions. $\vec{n}$ denotes the outward unit normal vector on Γ_o.

The parameters of the flow are the kinematic viscosity $\nu > 0$ and the Dirichlet boundary condition $\vec{g}$. Note that (5) is called the variational "do-nothing" or variational "free-stream" boundary condition, since it does not prescribe anything at Γ_o. It can be derived from a variational setting of the momentum equation (1). The inflow boundary condition $\vec{g}$ is modelled by a Poiseuille profile centred at $(0, 0)$, i.e.,

$$\vec{g}(\vec{x}) := \vec{g}(x_1, x_2, 0) := -U_{max}(1 - (x_1^2 + x_2^2)/L^2)\vec{e}_3, \quad x_1^2 + x_2^2 \leq L^2, \tag{6}$$

where $\vec{x} := (x_1, x_2, x_3)$, and $\vec{e}_3 := (0, 0, 1)$. $L > 0$ denotes the radius of the circular inflow boundary, and $U_{max} > 0$ corresponds to the maximum absolute value of the profile in $-\vec{e}_3$ direction. The rotor has diameter $D = 0.052[m]$ for which we assume a fixed angular speed $\omega > 0$ with axis of rotation $\vec{e}_3$. The dynamics of the flow can be characterized by the Reynolds number Re, defined as

$$Re := \frac{\omega D^2}{\nu}. \tag{7}$$

2.1 Multiple reference frame method (MRF)

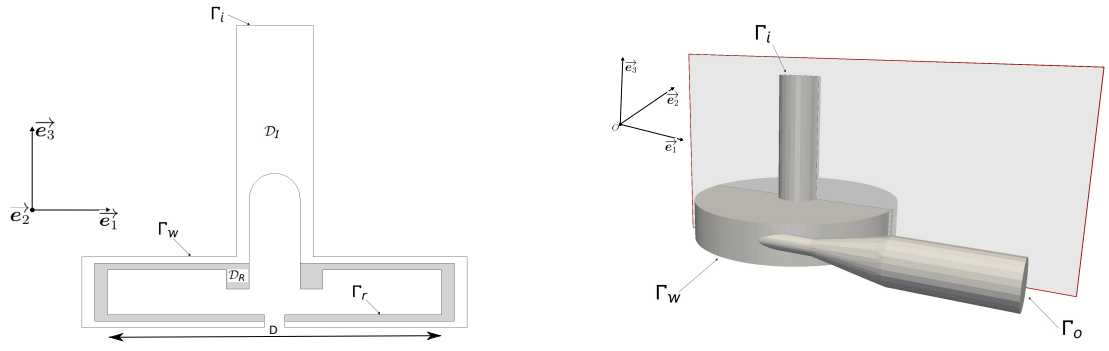

(a) 2d cross section showing a slice of the rotor.

(b) 3d surface with cutting plane for (a).

Figure 1: Geometry of the blood pump. The reference domain for the MRF method $\mathcal{D}_R$ is highlighted in (a).

A part of the domain $\mathcal{D}$ is moving in time due to the rotation of the rotor. Our goal is to map the rotation to the equations (1)–(5), and solve them on a stationary reference system. To this

end, we split $\mathcal{D}$ into two parts: $\mathcal{D}_I$ and $\mathcal{D}_R$ (compare Figure 1). On $\mathcal{D}_I$ an inertial coordinate system is used, which does not require any modification to (1)–(5). For $\mathcal{D}_R$ we define a reference velocity $\vec{u}_R$ by

$$\vec{u}_R = \vec{u} - \omega\vec{e}_3 \times \vec{x}, \tag{8}$$

for $\vec{x} \in \mathcal{D}_R$. Since the reference domain is stationary, we need to prescribe additional forces in the momentum equation to take into account the movement of the domain $\mathcal{D}_R$. We assume a time-independent angular speed, i.e., $\dot{\omega} = 0$. Therefore, including a coriolis force $2\omega\vec{e}_3 \times \vec{u}_R(\vec{x})$ and a centrifugal force $\omega^2\vec{e}_3 \times \vec{e}_3 \times \vec{x}$ in the momentum equation is sufficient (no Euler force required). The modified equations read:

$$\begin{aligned}
(\vec{u}_R(\vec{x}) \cdot \nabla)\vec{u}_R(\vec{x}) + 2\omega\vec{e}_3 \times \vec{u}_R(\vec{x}) + \omega^2\vec{e}_3 \times \vec{e}_3 \times \vec{x} & \\
-\nu\Delta\vec{u}_R(\vec{x}) + \nabla p(\vec{x}) = 0, \qquad & \vec{x} \in \mathcal{D}_R, \qquad (9)\\
\nabla \cdot \vec{u}_R(\vec{x}) = 0, \qquad & \vec{x} \in \mathcal{D}_R, \qquad (10)\\
\vec{u}_R(\vec{x}) = \vec{h}(\vec{x}), \qquad & \vec{x} \in \Gamma_r. \qquad (11)
\end{aligned}$$

Here, $\Gamma_r \subset \partial\mathcal{D}_R$ denotes the boundary on the rotor on which the rotation of the flow is prescribed by a Dirichlet boundary condition (compare Figure 1). Specifically, we define

$$\vec{h}(\vec{x}) := \vec{h}(x_1, x_2, 0) := \begin{bmatrix} -\omega x_2 \\ \omega x_1 \\ 0 \end{bmatrix} = \omega\vec{e}_3 \times \vec{x}. \tag{12}$$

Note that no boundary condition needs to be prescribed at the intersection of $\mathcal{D}_I$ and $\mathcal{D}_R$. The coupling between these two domains is provided in a natural way, since the reference geometry is not moving, therefore the associated finite element mesh connects the corresponding degrees of freedom. T his can be incorporated easily for assembling the stiffness matrix by introducing marks for each domain and checking their value within the assembly routine to choose the correct set of equations.

2.2 Uncertainty model

The flow equations are allowed to have three different sources of parametric uncertainty: 1) the Dirichlet boundary condition $\vec{g}$, 2) the angular speed ω, and 3) the kinematic viscosity ν. We model each of them by independent, uniformly distributed random variables $\xi_i \sim U(-1, 1)$, $i = 1, 2, 3$ such that

$$\vec{g}(x) = \vec{g}_0(x) + \sigma_1\vec{g}_0(x)\xi_1, \quad x \in \Gamma_i \tag{13}$$

$$\omega = \omega_0 + \sigma_2\omega_0\xi_2, \tag{14}$$

$$\nu = \nu_0 + \sigma_3\nu_0\xi_3. \tag{15}$$

In order to ensure positivity, we assume that the variation factors σ_i satisfy $0 < \sigma_i < 1$ for $i = 1, 2, 3$. The mean $\vec{g}_0$ of the Dirichlet boundary condition is defined as the Poiseuille profile introduced in (6). We combine the random variables in one random vector $\xi := (\xi_1, \xi_2, \xi_3)$. By using ξ we actually map an abstract probability space $(\Omega, \mathcal{A}, \mathbb{P})$ with sample space Ω, sigma-algebra $\mathcal{A} \subseteq 2^\Omega$, and probability measure $\mathbb{P}$ to the subset $\Xi \subseteq \mathbb{R}^3$, which along with the probability distribution of ξ and a corresponding Borel set also defines a probability space. We therefore do not need to pose our problem in terms of Ω, we rather can express all stochastic quantities in terms of ξ. Note that this results in an additional explicit dependence of the velocity and pressure variables on ξ.

2.3 Stochastic Galerkin projection

We employ a Polynomial Chaos (PC) expansion for the velocity and pressure components of the flow [28, 29]. Specifically, we expand these quantities in terms of an infinite series using orthogonal polynomials in ξ:

$$\vec{u}(\vec{x},\xi) = \sum_{i=0}^{\infty} \vec{u}_i(\vec{x})\psi_i(\xi), \quad p(\vec{x},\xi) = \sum_{i=0}^{\infty} p_i(\vec{x})\psi_i(\xi), \tag{16}$$

where we assume that $\vec{u}$ and p are square-integrable with respect to ξ point wise in $\vec{x}$, i.e., $\vec{u}(\vec{x}), p(\vec{x}) \in L^2(\Xi)$. $\{\psi_i\}_{i=0}^{\infty}$ denote the Chaos Polynomials, which in our case correspond to normalized Legendre Polynomials. These are orthogonal with respect to the constant probability density function of ξ, i.e.,

$$\int_{[-1,1]^3} \psi_i(\xi)\psi_j(\xi)\frac{1}{2^3}\, d\xi = \delta_{ij}, \tag{17}$$

where δ_{ij} denotes the Kronecker delta function, i.e., $\delta_{ij} = 0$, if $i \neq j$, $\delta_{ii} = 1$ otherwise. Since infinite sums are not feasible for numerical computation a truncation is employed by prescribing a maximum total polynomial degree $d \in \mathbb{N}$ such that

$$\vec{u}(\vec{x},\xi) \approx \sum_{i=0}^{P} \vec{u}_i(\vec{x})\psi_i(\xi), \quad p(\vec{x},\xi) \approx \sum_{i=0}^{P} p_i(\vec{x})\psi_i(\xi), \tag{18}$$

where $P + 1 = (d + 3)!/(d!3!)$. For a convergence analysis regarding the classical formulation of Polynomial Chaos in the Gaussian case see [5]. The generalized case is treated in [8].

We discretize the stochastic space by the stochastic Galerkin projection, see for example [15]. We illustrate the procedure on the set of equations (9)–(11) on the reference domain. In a similar way, the same procedure can be applied to the system (1)–(5) as well. First, the truncated PC expansions are inserted into the equations (9)–(11), resulting in:

$$\begin{aligned} &\sum_{i,j=0}^{P} (\vec{u}_{R,i}\cdot\nabla)\vec{u}_{R,j}\psi_i\psi_j + \sum_{i,j=0}^{P} 2\omega_i\vec{e}_3\times\vec{u}_{R,j}\psi_i\psi_j \\ &+ \sum_{i,j=0}^{P} \omega_i\omega_j\vec{e}_3\times\vec{e}_3\times\vec{x}\psi_i\psi_j - \sum_{i,j=0}^{P} \nu_i\Delta\vec{u}_{R,j}\psi_i\psi_j + \sum_{i=0}^{P} \nabla p_i\psi_i = 0, \end{aligned} \tag{19}$$

$$\sum_{i=0}^{P} \nabla\cdot\vec{u}_{R,i}\psi_i = 0, \tag{20}$$

$$\sum_{i=0}^{P} \vec{u}_{R,i}\psi_i = (\omega_0\psi_0 + \omega_2\psi_2)\vec{e}_3\times\vec{x}, \tag{21}$$

where we stopped noting the dependence of the velocity and pressure components on $\vec{x}$ and ξ for notational convenience. We artificially define

$$\omega_i := 0,\ i \neq 0, 2,\ \omega_2 := \sigma_2\omega_0, \quad \nu_i := 0,\ i \neq 0, 3,\ \nu_3 := \sigma_3\nu_0 \tag{22}$$

for ease of illustration. Note that by definition we have $\psi_0(\xi) = 1$, $\psi_1(\xi) = \xi_1$, $\psi_2(\xi) = \xi_2$, and $\psi_3(\xi) = \xi_3$. Now the resulting system gets multiplied by some ψ_k, $k = 0, \ldots, P$, and the L^2

inner product on $L^2(\Xi)$ denoted by $\langle \cdot, \cdot \rangle$ is taken on the equations. Using the orthogonality of the polynomials we arrive at the discretized system:

$$\sum_{i,j=0}^{P} (\vec{u}_{R,i} \cdot \nabla)\vec{u}_{R,j} c_{ijk} + \sum_{i,j=0}^{P} 2\omega_i \vec{e}_3 \times \vec{u}_{R,j} c_{ijk}$$
$$+ \sum_{i,j=0}^{P} \omega_i \omega_j \vec{e}_3 \times \vec{e}_3 \times \vec{x} c_{ijk} - \sum_{i,j=0}^{P} \nu_i \Delta \vec{u}_{R,j} c_{ijk} + \nabla p_k = 0, \qquad \vec{x} \in \mathcal{D}_R \tag{23}$$
$$\nabla \cdot \vec{u}_{R,k} = 0, \qquad \vec{x} \in \mathcal{D}_R \tag{24}$$
$$\vec{u}_{R,k} = \omega_k \vec{e}_3 \times \vec{x}, \qquad \vec{x} \in \Gamma_r \tag{25}$$

for $k = 0, \ldots, P$, and $c_{ijk} := \langle \psi_i \psi_j, \psi_k \rangle$.

In summary, the following set of equations need to be solved on $\mathcal{D}_I$ and $\mathcal{D}_R$, respectively:

$$\sum_{i,j=0}^{P} (\vec{u}_i \cdot \nabla)\vec{u}_j c_{ijk} - \sum_{i,j=0}^{P} \nu_i \Delta \vec{u}_j c_{ijk} + \nabla p_k = 0, \qquad \vec{x} \in \mathcal{D}_I \tag{26}$$
$$\nabla \cdot \vec{u}_k = 0, \qquad \vec{x} \in \mathcal{D}_I \tag{27}$$
$$\vec{u}_k = \langle \vec{g}(x), \psi_k \rangle, \qquad \vec{x} \in \Gamma_i \tag{28}$$
$$\vec{u}_k(\vec{x}) = 0, \qquad \vec{x} \in \Gamma_w, \tag{29}$$
$$\sum_{i,j=0}^{P} \int_{\Gamma_o} \nu_i \nabla \vec{u}_j(\vec{x}) \cdot \vec{n}(\vec{x}) c_{ijk} - p_k(\vec{x}) \vec{n}(\vec{x}) \, d\vec{x} = 0. \tag{30}$$
$$\sum_{i,j=0}^{P} (\vec{u}_i \cdot \nabla)\vec{u}_j c_{ijk} + \sum_{i,j=0}^{P} 2\omega_i \vec{e}_3 \times \vec{u}_j c_{ijk}$$
$$+ \sum_{i,j=0}^{P} \omega_i \omega_j \vec{e}_3 \times \vec{e}_3 \times \vec{x} c_{ijk} - \sum_{i,j=0}^{P} \nu_i \Delta \vec{u}_j c_{ijk} + \nabla p_k = 0, \qquad \vec{x} \in \mathcal{D}_R \tag{31}$$
$$\nabla \cdot \vec{u}_k = 0, \qquad \vec{x} \in \mathcal{D}_R \tag{32}$$
$$\vec{u}_k = \omega_k \vec{e}_3 \times \vec{x}, \qquad \vec{x} \in \Gamma_r, \tag{33}$$

for $k = 0, \ldots, P$. Note that since the equations are posed on a stationary reference system, we do not need to distinguish between reference variables $\vec{u}_R,\ p_R$ and inertial variables $u,\ p$ in equations (26)–(33). We continue with a brief discussion of our used solvers in the following section.

3 NUMERICAL METHODS

The quadratic non-linearity in the convective term of the momentum equations (26) and (31) is linearised using Newton's method. In each Newton iteration a linear system needs to be solved for $\vec{u}$ and p given some linearisation point $\vec{v}$ and q. The corresponding momentum and

mass equations read:

$$\sum_{i,j=0}^{P}(\vec{u}_j\cdot\nabla)\vec{v}_i c_{ijk}+\sum_{i,j=0}^{P}(\vec{v}_i\cdot\nabla)\vec{u}_j c_{ijk}-\sum_{i,j=0}^{P}\nu_i\Delta\vec{u}_j c_{ijk}+\nabla p_k=-r(\vec{v},q),\quad \vec{x}\in\mathcal{D}_I, \tag{34}$$

$$\sum_{i,j=0}^{P}(\vec{u}_j\cdot\nabla)\vec{v}_i c_{ijk}+\sum_{i,j=0}^{P}(\vec{v}_i\cdot\nabla)\vec{u}_j c_{ijk}$$

$$+\sum_{i,j=0}^{P}2\omega_i\vec{e}_3\times\vec{u}_j c_{ijk}-\sum_{i,j=0}^{P}\nu_i\Delta\vec{u}_j c_{ijk}+\nabla p_k=-r(\vec{v},q),\quad \vec{x}\in\mathcal{D}_R, \tag{35}$$

$$\nabla\cdot\vec{u}_k=-\nabla\cdot\vec{v}_k,\quad \vec{x}\in\mathcal{D}, \tag{36}$$

where the momentum residual $r(\vec{v},q)$ is defined as the evaluation of (26) and (31) at the velocity $\vec{v}$ and pressure q given by the Newton iteration. The next Newton iterates, say $\vec{u}_{new}$ and p_{new} are given by $\vec{u}_{new}:=\vec{v}+\vec{u},\ p_{new}:=q+p$.

The spatial part of equations (34)–(36) is discretized by the finite element method using Lagrangian Taylor-Hood elements of degree two and one for the velocity and pressure PC coefficients, respectively [26].

3.1 Mean based preconditioner

After discretization of the spatial part, we obtain a linear system of equations for the Newton system (34)–(36). We use a Krylov subspace method to compute its solution. Specifically, we employ the generalized minimal residual method (GMRES [21]). Choosing a good preconditioner is crucial to speed up the convergence of GMRES. In [18, 19] a mean based preconditioner has been analysed, which is effective if the stochastic variations σ_i, $i=1,2,3$ do not become too large.

The stiffness matrix $A(\vec{v})\in\mathbb{R}^{(P+1)N,(P+1)N}$ associated to a finite-element discretization using N degrees of freedom of equations (34)–(36) at linearisation point $\vec{v}$ can be written in terms of the Kronecker product:

$$A(\vec{v})=\sum_{i=0}^{P}G_i\otimes A_i(\vec{v}), \tag{37}$$

where $A_i(\vec{v})\in\mathbb{R}^{N,N}$, $i=0,\dots,P$ denote the Kronecker factors and $G_i\in\mathbb{R}^{P+1,P+1}$, $i=0,\dots,P$ denote the stochastic Galerkin matrices defined by $(G_i)_{j,k}:=c_{ijk}$. The Kronecker factors $A_i(\vec{v})$ can be extracted from equations (34)–(36). A Kronecker factor $A_i(\vec{v})$ corresponds to the finite element discretization of:

$$(\vec{u}\cdot\nabla)\vec{v}_i+(\vec{v}_i\cdot\nabla)\vec{u}-\nu_i\Delta\vec{u}+\nabla p,\qquad \vec{x}\in\mathcal{D}_I, \tag{38}$$

$$(\vec{u}\cdot\nabla)\vec{v}_i+(\vec{v}_i\cdot\nabla)\vec{u}+2\omega_i\vec{e}_3\times\vec{u}-\nu_i\Delta\vec{u}+\nabla p,\qquad \vec{x}\in\mathcal{D}_R, \tag{39}$$

$$\nabla\cdot\vec{u},\qquad \vec{x}\in\mathcal{D}, \tag{40}$$

where $\vec{u}$ and p represent deterministic velocity and pressure variables associated to $A_i(\vec{v})=A_i(\vec{v}_i)$. The mean based preconditioner B is then defined as

$$B:=I\otimes A_0(\vec{v})=I\otimes A_0(\vec{v}_0), \tag{41}$$

which has the attractive feature that it is block-diagonal and therefore applicable in a decoupled way with respect to the stochastic space. This gives a natural parallelism in the preconditioning step.

3.2 Multilevel method

As an alternative to using Krylov subspace methods for solving the linear system of equations for the Newton system (34)–(36) we consider a multilevel approach, which is inspired by multigrid algorithms for deterministic problems. It has already been successfully applied to elliptic equations with random parameters in [20, 23].

The Polynomial Chaos expansion presents a natural hierarchy with respect to the total polynomial degree. Let $\mathcal{S}_d$ denote the space spanned by the Chaos Polynomials up to the total degree $d \in \mathbb{N}$, i.e.,

$$\mathcal{S}_d := span\{\psi_0, \dots, \psi_{P_d}\}, \tag{42}$$

with $P_d + 1 = (d+M)!/(d!M!)$, where M denotes the dimension of ξ, i.e., in our case $M = 3$. We can express the hierarchy by a nested sequence of spaces

$$\mathcal{S}_0 \subseteq \mathcal{S}_1 \subseteq \cdots \subseteq \mathcal{S}_d. \tag{43}$$

Given some total degree d suppose we can write the spatially discretized Newton step (34)–(36) in the following way:

$$\sum_{i=0}^{P_d} (G_i \otimes A_i) y^d = -b^d, \tag{44}$$

with $y^d,\ b^d \in \mathbb{R}^{(P_d+1)N}$ denoting the solution and residual vector in the Newton system. Here, we assume N degrees of freedom for the finite element discretization. We stopped noting the dependence of A_i on the linearisation vector $\vec{v}$ for notational convenience. We can adapt the idea from deterministic multigrid algorithms to the nested subspace structure given in (42) with "grid level" d. To exchange information between different levels, we define a restriction operator $\mathcal{R}_{d-1}$ as the L^2 projection of $\mathcal{S}_d$ onto $\mathcal{S}_{d-1}$, and a prolongation operator $\mathcal{P}_d$ as a natural inclusion operator from $\mathcal{S}_{d-1}$ to $\mathcal{S}_d$. As a smoothing operator we employ θ iterations of the mean based preconditioner, i.e., given an initial iterate y_0^d we perform θ iterations of the following form:

$$y_{k+1}^d := \mathcal{B}_d y_k^d := y_k^d + (I_d \otimes A_0)^{-1}(b^d - \sum_{i=0}^{P_d} (G_i \otimes A_i) y_k^d), \tag{45}$$

where k is the iteration index, and I_d denotes the identity matrix of dimension $P_d + 1$. For $d = 0$ we obtain the mean problem $A_0 y^0 = b^0$. A brief overview of the multilevel method is provided in Figure 2. Note that in the multilevel method only solutions to the mean operator A_0 need to be computed if full cycles (down to $d = 0$) are used.

4 NUMERICAL RESULTS

We use the inexact Newton method for solving the non-linear system in (26)–(33). In contrast to the classical Newton method, it only requires approximate solutions within each Newton step in order to obtain convergence. Thereby, we employ the strategy "choice 1" of Eisenstat and Walker [7] with initial "forcing term" equal to 0.5, i.e., the first Newton system needs to be solved to a relative accuracy of 0.5. The relative accuracy is then decreased for each following Newton iteration by the "choice 1" strategy.

For the solution of the linear systems arising in the Newton iterations we employ the GMRES and Multilevel (ML) method as described in the previous section. Since both methods require multiple solves with respect to the mean operator A_0 – either for the preconditioner in GMRES or the smoothing operator in ML – we need to define an "inner" solver for these systems as well.

1: **if** $(d = 0)$ **then**
2: solve $A_0 y^0 = b^0$ (system size N)
3: **else**
4: $y^d = \mathcal{B}_d^\theta y^d$ (pre-smoothing, θ times)
5: $r^d := b^d - \sum_{i=0}^{P_d} (G_i \otimes A_i) y^d$ (compute linear residual on level d)
6: $r^{d-1} = \mathcal{R}_{d-1} r^d$ (restrict residual to level $d-1$)
7: **for** $m = 0$ **to** $m < \mu$ **do**
8: ML$(c^{d-1}, r^{d-1}, d-1)$ (correction computation on level $d-1$, μ times)
9: **end for**
10: $c^d = \mathcal{P}_d c^{d-1}$ (prolongate correction to level d)
11: $y^d = y^d + c^d$ (update solution with correction on level d)
12: $y^d = \mathcal{B}_d^\theta y^d$ (post-smoothing, θ times)
13: **end if**

Figure 2: One cycle of the multilevel method: ML(y^d, b^d, d) given a vector y^d and right hand side b^d on level d. $\mu = 1$ results in a V-cycle, $\mu = 2$ in a W-cycle.

Inflow maximal speed (m/s)	0.55	Inflow speed variation (σ_1)	10%
Dynamic viscosity $(N \cdot s/m^2)$	0.0035	Viscosity variation (σ_3)	10%
Angular speed (rad/s)	261.8	Angular speed variation (σ_2)	10%
RPM	2500	Density (Kg/m^3)	1.035

Table 1: Model parameter values.

We again rely on the GMRES method with incomplete LU preconditioning for that case, which should not be confused with the "outer" GMRES solver for the stochastic Galerkin system. Since A_0 omits a saddle point structure, we apply the LU factorization on the upper left diagonal block of the matrix A_0.

Furthermore, we analyse two variants of the ML method, the first one of which solves each system with A_0 to a relative accuracy below 10^{-12}, while the second one uses a relative accuracy of 10^{-1}. We denote these two variants by ML$_{exact}$ and ML$_{appr}$, respectively. The relative error tolerances for the "outer" solvers, GMRES and ML, are provided by the inexact Newton method, which itself is iterating until an absolute or relative error is achieved below 10^{-9}.

As described in section 2.2, we consider three independent and uniformly distributed uncertain parameters in our numerical model: the inflow boundary velocity, the kinematic viscosity and the rotor's angular speed. Their values and stochastic variation factors are provided in Table 1. As defined in section 2 this results in a mean Reynolds number $Re \approx 200$. We compare three different total polynomial degrees ($d = 3$, $d = 4$ and $d = 5$) for the PC expansion, which result in 20, 35 and 56 PC modes for the velocity and pressure variables, respectively. The discretization of the spatial component is done by Lagrangian finite elements with degree 2 for the velocity and degree 1 for the pressure PC modes. This results in 919,334 degrees of freedom per PC mode (for both velocity and pressure) using a finite element mesh with 192,451 cells.

Table 2 provides a comparison of the computational cost associated to each method. We first compare GMRES with ML$_{exact}$. Both methods perform similar in terms of number of iterations, while ML$_{exact}$ demonstrates a slightly more robust convergence behaviour. However, ML$_{exact}$ requires more solutions to the mean operator A_0, more evaluations of residuals and more iterations in average for the solution of the mean systems associated to A_0. The

		Newton iter. ($d = 3$)				**Newton iter.** ($d = 4$)			**Newton iter.** ($d = 5$)		
		1	**2**	**3**	**4**	**1**	**2**	**3**	**1**	**2**	**3**
GMRES	N_{iter}	1	2	3	-	1	2	3	1	2	3
	N_{res}	2	3	4	-	2	3	4	2	3	4
	N_{A_0}	23	60	80	-	23	102	140	23	136	224
	$\overline{N}_{iter,A_0}$	706	931	967	-	706	755	933	706	619	893
ML$_{exact}$	N_{iter}	1	1	1	-	1	1	2	1	1	1
	N_{res}	11	11	11	-	14	14	27	17	17	17
	N_{A_0}	55	68	67	-	107	139	278	180	251	251
	$\overline{N}_{iter,A_0}$	758	1380	1804	-	715	1307	919	600	1093	1346
ML$_{appr}$	N_{iter}	1	1	3	2	1	1	3	1	1	1
	N_{res}	11	11	31	21	14	14	40	17	17	33
	N_{A_0}	57	69	207	138	108	139	417	183	251	502
	$\overline{N}_{iter,A_0}$	63	95	137	338	49	75	107	41	63	102

Table 2: Comparison of 3 different polynomial degrees of the PC expansion. N_{iter} denotes the number of GMRES iterations or V-cycles, respectively. N_{res} denotes the number of residual computations, N_{A_0} denotes the number of systems, which need to be solved with the mean matrix A_0, and $\overline{N}_{iter,A_0}$ denotes the averaged number of GMRES iterations, which are required to compute solutions with A_0. The average is taken in each Newton iteration over all system solves associated to A_0.

increase in computational effort with respect to the Newton iteration is related to the inexact Newton approach, which decreases the relative error tolerances in each iteration and therefore requires more iterations in each Newton step. In contrast, ML$_{appr}$ outperforms both GMRES and ML$_{exact}$. Although for $d = 3$ one additional Newton iteration is required for ML$_{appr}$, the dominant computational cost is significantly lower. We measure this cost in terms of C_s, which is defined as the product of the number of system solves associated to A_0 and the average number of GMRES iterations used for A_0, i.e., $C_s = N_{A_0}\overline{N}_{iter,A_0}$ as defined in Table 2. The savings in computational cost are highlighted in Fig. 3.

Figure4 depicts the mean of the solution for the pressure and velocity. The highest pressure can be observed in the area of inlet because of the prescribed inflow boundary condition for the velocity. Within the rotor segment the pressure is varying on both sides due to Coriolis and centrifugal forces. As expected, the velocity around the blade's outer edge (near to rim) is

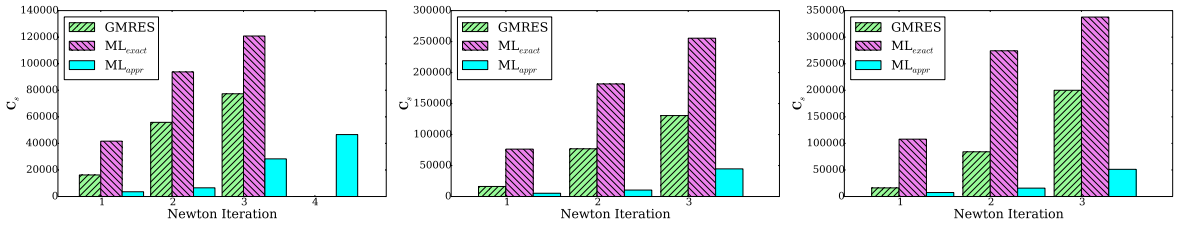

(a) PC degree $d = 3$. (b) PC degree $d = 4$. (c) PC degree $d = 5$.

Figure 3: Comparison of the computational cost of GMRES, ML$_{exact}$ and ML$_{appr}$.

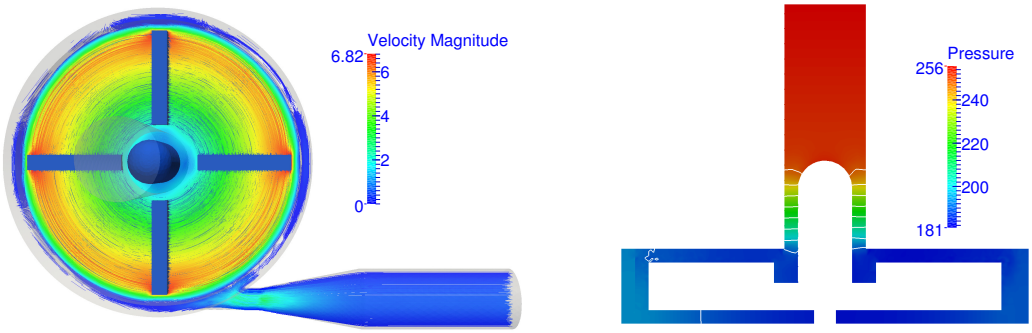

(a) Streamlines and velocity magnitude.

(b) Mean value of pressure.

Figure 4: Mean of the flow profile and pressure.

much higher than in the area around the hub. Overall, the mean of the flow demonstrates a stable laminar behaviour, which has been verified with deterministic reference computations. To this end, we computed the l_2 difference between each deterministic reference and the corresponding stochastic point evaluation of the PC expansion of the stochastic solution at various points in the stochastic domain. The maximum of these errors was slightly below 10^{-6} for the case $d = 3$ with smaller values for larger polynomial degrees of the PC expansion.

In Figure 5 we depict the standard deviation of the velocity components and the pressure variable. For the pressure, most uncertainty has impact on the inlet part, while for the $\vec{e}_1$ and $\vec{e}_2$ component of the velocity the dominant uncertainty is close to the rim in the rotor domain. Note that only minor uncertainty can be observed in the outlet part. We expect this to increase significantly for a higher Reynolds number flow.

5 CONCLUSIONS

We presented a numerical simulation of a bloop pump with uncertain parameters. To this end, we showed how to adapt the Multiple Reference Frame method to transfer the uncertain angular speed of the rotor to the governing equations. This enables the use of the stochastic Galerkin projection with Polynomial Chaos for discretization of the dependence of the flow profile and pressure on the uncertain parameters.

We focused on a stabilized flow by artificially increasing the kinematic viscosity of the fluid. This results in a steady state laminar flow regime, which can be used as an initial iterate for an unsteady simulation for higher Reynolds numbers. We analysed three different numerical solution methods, GMRES, exact Multilevel and approximate Multilevel. While GMRES displayed faster convergence than exact Multilevel, the approximate version clearly outperformed the other two with significantly less numerical cost. In addition, we verified our results against deterministic reference solutions, which showed high accuracy even for a third order PC expansion. In principle, the proposed methods can be reused for other stochastic fluid flow problems as well.

Our current work is focused on the extension of the CFD analysis to the time-dependent case for higher Reynolds number flows. Although, we employed the stochastic Galerkin projection in this work, the computed PC expansion of the flow profile and pressure can be evaluated at any point in the parameter space. Therefore, in the unsteady case both the stochastic Galerkin projection and non-intrusive methods can reuse the computed solution.

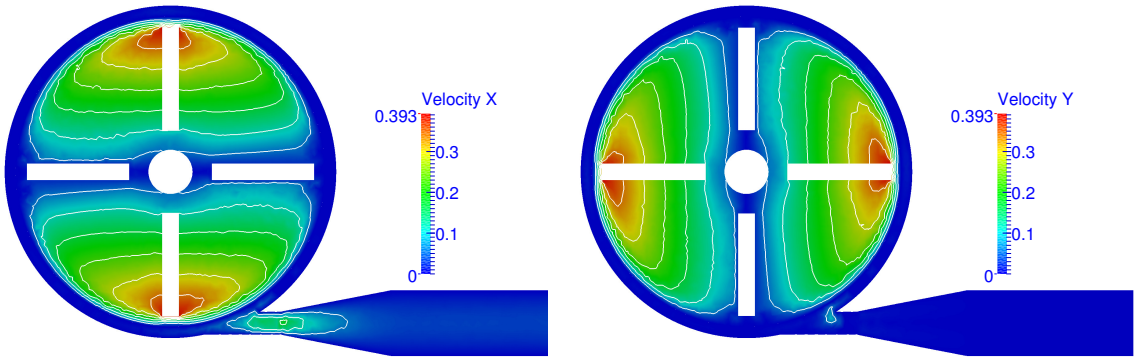

(a) Standard deviation of velocity in direction $\vec{e}_1$. (b) Standard deviation of velocity in direction $\vec{e}_2$.

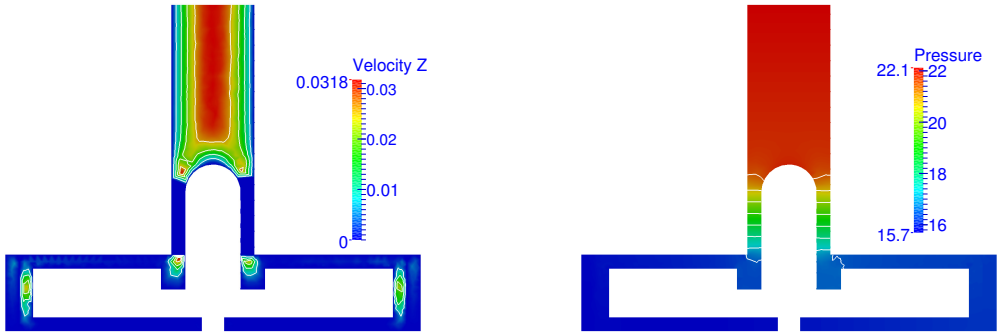

(c) Standard deviation of velocity in direction $\vec{e}_3$. (d) Standard deviation of pressure.

Figure 5: Standard deviations for the flow profile and pressure.

REFERENCES

[1] Computational fluid dynamics: An FDA critical path initiative. `https://fdacfd.nci.nih.gov/interlab_study_2_blood_pump`, 2013.

[2] Emma J Birks, Patrick D Tansley, James Hardy, Robert S George, Christopher T Bowles, Margaret Burke, Nicholas R Banner, Asghar Khaghani, and Magdi H Yacoub. Left ventricular assist device and drug therapy for the reversal of heart failure. *New England Journal of Medicine*, 355(18):1873–1884, 2006.

[3] W. Bujalski, Z. Jaworski, and A.W. Nienow. CFD study of homogenization with dual rushton turbinescomparison with experimental results: Part ii: The multiple reference frame. *Chemical Engineering Research and Design*, 80(1):97 – 104, 2002. Process and Product Development.

[4] Daniel Burkhoff, Howard Cohen, Corinna Brunckhorst, and William W. O'Neill. A randomized multicenter clinical study to evaluate the safety and efficacy of the tandemheart percutaneous ventricular assist device versus conventional therapy with intraaortic balloon pumping for treatment of cardiogenic shock. *American Heart Journal*, 152(3):469.e1 – 469.e8, 2006.

[5] R.H. Cameron and W.T. Martin. The orthogonal development of non-linear functionals in series of Fourier-Hermite functionals. *The Annals of Mathematics*, 48(2):385–392, 1947.

[6] S.M.A. Cruz, A.J.M. Cardoso, and H.A. Toliyat. Diagnosis of stator, rotor and airgap eccentricity faults in three-phase induction motors based on the multiple reference frames theory. In *Industry Applications Conference, 2003. 38th IAS Annual Meeting. Conference Record of the*, volume 2, pages 1340–1346 vol.2, Oct 2003.

[7] Stanley C. Eisenstat, Homer F. Walker, Stanley C. Eisenstatt, Homer, and F. Walker. Choosing the forcing terms in an inexact newton method. *SIAM J. Sci. Comput*, 17:16–32, 1994.

[8] Oliver G. Ernst, Antje Mugler, Hans-Jörg Starkloff, and Elisabeth Ullmann. On the convergence of generalized polynomial chaos expansions. *ESAIM: Mathematical Modelling and Numerical Analysis*, 46(2):317–339, 2012.

[9] O.H. Frazier, Richard K. Wampler, J.Michael Duncan, Wayne E. Dear, Michael P. Macris, Steven M. Parnis, and John M. Fuqua. First human use of the hemopump, a catheter-mounted ventricular assist device. *The Annals of Thoracic Surgery*, 49(2):299 – 304, 1990.

[10] Roger Ghanem and P. D. Spanos. *Stochastic finite elements: A spectral approach*. Springer-Verlag New York, NY, 1991.

[11] F. Kerdouss, A. Bannari, and P. Proulx. CFD modeling of gas dispersion and bubble size in a double turbine stirred tank. *Chemical Engineering Science*, 61(10):3313 – 3322, 2006.

[12] O.M. Knio and O. P. Le Maître. Uncertainty propagation in CFD using Polynomial Chaos decomposition. *Fluid Dynamics Research*, 38:616–640, 2006.

[13] P.C. Krause. Method of multiple reference frames applied to the analysis of symmetrical induction machinery. *Power Apparatus and Systems, IEEE Transactions on*, PAS-87(1):218–227, Jan 1968.

[14] Olivier P. Le Maître, Omar M. Kino, Habib N. Najm, and Roger G. Ghanem. A stochastic projection method for fluid flow. I: basic formulation. *J. Comput. Phys.*, 173:481–511, 2001.

[15] Olivier P. Le Maître and Omar M. Knio. *Spectral Methods for Uncertainty Quantification : With Applications to Computational Fluid Dynamics*. Springer Science+Business Media B.V, Dordrecht, 2010.

[16] F. Nobile, R. Tempone, and C.G. Webster. An anisotropic sparse grid stochastic collocation method for partial differential equations with random input data. *SIAM Journal on Numerical Analysis*, 46(5):2411–2442, 2008.

[17] Francis D. Pagani, Leslie W. Miller, Stuart D. Russell, Keith D. Aaronson, Ranjit John, Andrew J. Boyle, John V. Conte, Roberta C. Bogaev, Thomas E. MacGillivray, Yoshifumi Naka, Donna Mancini, H. Todd Massey, Leway Chen, Charles T. Klodell, Juan M. Aranda, Nader Moazami, Gregory A. Ewald, David J. Farrar, and O. Howard Frazier. Extended mechanical circulatory support with a continuous-flow rotary left ventricular assist device. *Journal of the American College of Cardiology*, 54(4):312 – 321, 2009.

[18] M.F Pellissetti and R.G Ghanem. Iterative solution of systems of linear equations arising in the context of stochastic finite elements. *Advances in Engineering Software*, 31(89):607 – 616, 2000.

[19] Catherine E. Powell and Howard C. Elman. Block-diagonal preconditioning for spectral stochastic finite-element systems. *IMA Journal of Numerical Analysis*, 29(2):350–375, 2009.

[20] Eveline Rosseel and Stefan Vandewalle. Iterative Solvers for the stochastic Finite Element Method. *SIAM J. Sci. Comput.*, 32:372–397, 2010.

[21] Youcef Saad and Martin H Schultz. GMRES: A generalized minimal residual algorithm for solving nonsymmetric linear systems. *SIAM J. Sci. Stat. Comput.*, 7(3):856–869, July 1986.

[22] M. Schick, Vincent Heuveline, and O.P. Le Maître. A newton-galerkin method for fluid flow exhibiting uncertain periodic dynamics. *SIAM/ASA Journal on Uncertainty Quantification*, 2(1):153–173, 2014.

[23] Michael Schick. A parallel multilevel spectral galerkin solver for linear systems with uncertain parameters. *2014 22nd Euromicro International Conference on Parallel, Distributed, and Network-Based Processing*, 0:352–359, 2014.

[24] D. J. Silvester and C. E. Powell. Preconditioning steady-state Navier-Stokes equations with random data. *SIAM J. Sci. Comput.*, 34(5), 2012.

[25] Mark S. Slaughter, Francis D. Pagani, Joseph G. Rogers, Leslie W. Miller, Benjamin Sun, Stuart D. Russell, Randall C. Starling, Leway Chen, Andrew J. Boyle, Suzanne Chillcott, Robert M. Adamson, Margaret S. Blood, Margarita T. Camacho, Katherine A. Idrissi, Michael Petty, Michael Sobieski, Susan Wright, Timothy J. Myers, and David J. Farrar. Clinical management of continuous-flow left ventricular assist devices in advanced heart failure. *The Journal of Heart and Lung Transplantation*, 29(4, Supplement):S1 – S39, 2010. Clinical Management of Continuous-flow Left Ventricular Assist Devices in Advanced Heart Failure.

[26] C. Taylor and P. Hood. A numerical solution of the navier-stokes equations using the finite element technique. *Computers & Fluids*, 1(1):73–100, 1973.

[27] Norbert Wiener. The homogeneous chaos. *American Journal of Mathematics*, 60(4):897–936, October 1938.

[28] Dongbin Xiu and George Em Karniadakis. The wiener–askey polynomial chaos for stochastic differential equations. *SIAM J. Sci. Comput.*, 24(2):619–644, February 2002.

[29] Dongbin Xiu and George Em Karniadakis. Modeling uncertainty in flow simulations via generalized polynomial chaos. *Journal of Computational Physics*, 187(1):137 – 167, 2003.